We are IntechOpen,
the world's leading publisher of
Open Access books
Built by scientists, for scientists

6,900
Open access books available

185,000
International authors and editors

200M
Downloads

154
Countries delivered to

Our authors are among the

TOP 1%
most cited scientists

12.2%
Contributors from top 500 universities

BOOK CITATION INDEX
CLARIVATE ANALYTICS
INDEXED

WEB OF SCIENCE™

Selection of our books indexed in the Book Citation Index
in Web of Science™ Core Collection (BKCI)

Interested in publishing with us?
Contact book.department@intechopen.com

Self-Consistent Micromechanical Enhancement of Continuous Fiber Composites

Andrew Ritchey[1], Joshua Dustin[1], Jonathan Gosse[2] and R. Byron Pipes[1]
[1]Purdue University
[2]The Boeing Company
USA

1. Introduction

Much of the previous work in developing analytical models for high performance composite materials has focused on representations of the heterogeneous medium as a homogenous, anisotropic continuum. The development of the equivalent properties of the homogenous medium from the geometry of the microstructure and the fiber and matrix properties has been come to be known as "micromechanics" (Daniel & Ishai, 2006). The term "homogenization" has been applied to the process of determining the effective properties of the homogenous medium and for much of the past half century homogenization was the only task of micromechanics. However, increases in computational capability has allowed for the use of micromechanics as a "de-homogenization" tool as well. The de-homogenization method that is the focus of the current study has been come to be known as "micromechanical enhancement" (Gosse & Christensen, 2001; Buchanan et al., 2009). Here the deformation of the homogeneous medium is enhanced by influence functions derived from unit cell micromechanical models representing extremes in the packing efficiencies of fiber arrangements. The motivation for development of the de-homogenization step is the need for an increase in the robustness and fidelity of failure theories used for these material systems wherein the deformation fields within the homogenized solutions are enhanced to reflect the actual strain field topologies within the fiber and matrix constituents. It is these enhanced strain fields that are used to determine the onset of damage initiation within the medium.

There are several categories of models which have been proposed to perform the homogenization step of micromechanics including: mechanics of materials (Voigt, 1887; Reuss, 1929); self-consistent field (Hill, 1965); bounding methods based on variation principals (Paul, 1960; Hashin & Rosen 1964); semi-empirical (Halpin & Tsai, 1967); numerical finite element methods (Sun & Vaidya, 1996) and experimental methods such as uniaxial coupon tests. A significant amount of work has been devoted to this topic and more complete reviews are found elsewhere (Christensen 1979; Pindera et al., 2009). Although any analysis method used should be vetted against a rigorous testing program, accurate micromechanics models can provide a cost effective method for a priori material evaluation and ranking of composite systems. In the traditional composite analysis workflow, homogenized material properties are used in a laminate analysis of a structural

member to determine lamina level stresses and strains. Stresses and strains at the lamina level are then used directly in a failure criterion to determine the ultimate performance of the member. Some success has been achieved with this approach but the analysis fails to take into account the actual state of stress and strain within the constituent phases. In addition, residual thermal stresses resulting from a mismatch in the coefficient of thermal expansion between the fiber and matrix phases are usually neglected. Others have noted that non-physical singularities may arise in homogenized solutions containing free-edges (Pagano & Rybicki, 1974; Pagano & Yuan, 2000).

Several methods for recovery of the state of stress/strain from a homogenized solution have been proposed as well. Analytic methods have been proposed base on phase averaging methods (Hill, 1963; Hashin 1972). More recently, numerical methods have been employed. One method is to perform a global-local finite element analysis. In this approach the forces or displacements obtained from a homogenized solution are applied to a domain in which the fiber and matrix phases are modelled explicitly (Wang et al., 2002). With this method one must first determine an appropriate size for the local region, typically containing several fibers, using the so-called "local domain test." It has been suggested that a single fiber local region is feasible for determining fiber-matrix interface stresses if the continuum is modelled using the micro-polar theory of elasticity (Hutapea et al., 2003). Others have suggested the use of a multilevel analysis that models a homogenized region, a transition region and a region containing the explicit microstructure in a single finite element analysis (Raghavan et al., 2001). A more computationally efficient method for recovering the stress and strain in the fiber and matrix phases is to use an influence function formulation (Gosse & Christensen, 2001). In this method, also referred to as mircomechanical enhancement, a set of six canonical states of deformation and a separate thermal load are applied to a unit cell prior to performing an analysis of the homogeneous medium. The influence functions extracted from the unit cells are then used to relate the state of homogenous strain in each lamina to the state of strain within the representative volume element through the use of the enhancement matrix. Microscopic residual thermal strains can also be recovered with a superposition vector (Buchanan et al., 2009).

In a previous study (Gosse & Christensen, 2001), the homogenization step was an experimental one wherein the effective properties of the homogenous medium employed in the analysis were determined by experiments while the de-homogenization (micromechanical enhancement) step was carried out by a finite element analysis of a representative volume element. In addition to this procedure, an alternative method has been developed to utilize the derived effective elastic and thermal lamina properties from the same micromechanical models developed to assessed the strain fields within the unit cells. In this paper the latter approach is investigated exclusively in order to provide the consistency of utilizing the same method for both homogenization and de-homogenization. In the current chapter, the micromechanical enhancement method is investigated in more detail and a self-consistent method for determining the microscopic strain field is presented. By using a self-consistent analysis, the inherent approximations of the method are present in both steps while no new uncertain quantities, such as experimental test variables, are introduced. Self-consistency is assured by utilizing the same micromechanical models for both the homogenization and de-homogenization steps in the method. The goal is to provide an efficient link in a multi-scale analysis of a composite structure and to elucidate the analysis steps used in the current method.

2. Homogenization

The homogenization process seeks to obtain equivalent homogenous continuum properties for a medium composed of multiple phases of varying constitutive properties. For the current discussion, we will limit ourselves to a heterogeneous medium consisting of collimated, continuous fibers within an isotropic matrix. Many methods and closed-form expressions have been developed to achieve this goal (Pindera et al., 2009). Among these, the most accurate in predicting the average response of an orthotropic medium is the finite element method (Daniel & Ishai, 2006). In the finite element approach, one would like to determine the relationship between the average stress and average strain as expressed in Equation 1.

$$\bar{\sigma}_i = \bar{C}_{ij}\left(\bar{\varepsilon}_j - \bar{\alpha}_j \Delta T\right) \ \left(i, j = 1-6\right) \tag{1}$$

The overbar indicates an average or homogenized quantity. From the homogenous stiffness matrix ($\bar{C}_{ij}$), the effective lamina engineering constants (E_1, E_2, v_{12}, G_{12}, etc.) can be calculated. Alternatively, the engineering constants can be determined directly by systematically performing finite element analysis corresponding to the definitions of the engineering constants (Sun & Vaidya, 1996). In this approach, the average stress is related to the average strain through the strain energy density. Typically, a representative volume element, as shown in Figure 1, is used to simplify the analysis. Equation 2 gives the stress-strain relation for the case when $\Delta T = 0$.

$$\bar{\sigma}_i = \bar{C}_{ij}\bar{\varepsilon}_j \ \left(i, j = 1-6\right) \tag{2}$$

Where "1" coincides with the fiber direction, "2" is transverse to the fiber direction and "3" is normal to the 1 and 2 directions. Also, note the use of a contracted notation such that i=1-3 are the three normal components of stress and strain, 11, 22, and 33, respectively, while i=4-6 are the three *engineering* shear components, 23, 13 and 12, respectively. The average stress is shown in Equation 3 for the case when a canonical state of deformation is applied so that the only active strain component is $\bar{\varepsilon}_1$. The superscript indicates the isolated average mechanical strain component. As shown, the relationship of can be rearranged to determine the first column of the homogenous stiffness matrix.

$$\bar{\sigma}_i^{(\bar{\varepsilon}_1)} = \bar{C}_{i1}^k \bar{\varepsilon}_1 \ \text{or} \ \bar{C}_{i1}^k = \bar{\sigma}_i^{(\bar{\varepsilon}_1)}\big/\bar{\varepsilon}_1 \ \left(i = 1-6\right) \tag{3}$$

The other five columns of the effective homogenous stiffness matrix are determined by applying the remaining five other states of canonical deformation such that each strain component is isolated. A total of six finite element analyses are required to fully determine the effective homogenous stiffness matrix for the general anisotropic solid. A seventh finite element analysis is required to determine the thermal response of the effective medium. For this case, the domain is subjected to a thermal loading of ΔT with the average mechanical strain, $\left\{\bar{\varepsilon} - \bar{\alpha}\Delta T\right\}$, constrained to be zero. Equation 4 gives the calculation of the average coefficients of thermal expansion. As seen from Equation 1, constraining the average mechanical strain to be zero requires that the average stress be zero. This condition can be used to check the validity of the boundary conditions.

$$\{\overline{\alpha}_i\} = \overline{\varepsilon}_i / \Delta T \quad (i = 1 - 6) \tag{4}$$

Equation 5 shows the average strain in a unit cell determined from the surface displacement, u_i and u_j with i,j = 1-3, by using Gauss' theorem and written in index notation (Sun & Vaidya, 1996).

$$\overline{\varepsilon}_{ij} = \frac{1}{2V} \int_S \left(u_i n_j + u_j n_i \right) dS \tag{5}$$

Where S is the boundary surface of the representative volume element and n_i is the unit surface normal in the ith direction. Thus, the average strain in the unit cell can be calculated for a set of displacement boundary conditions.

Specifying the components of deformation on the surface of the representative volume element will, in general, induce average stress components. The average stress is calculated in Equation 6 using the reaction forces obtained on the boundaries of the unit cell and the definition of stress.

$$\overline{\sigma}_{ij} = F_j n_i / A \quad (i, j = 1 - 3) \tag{6}$$

Where index notation is used with F_j the jth component of the total force applied to a face with a total area of A oriented in the ith direction. In this way, all six components of the stress tensor that may result for a state of deformation applied to the representative volume element are determined.
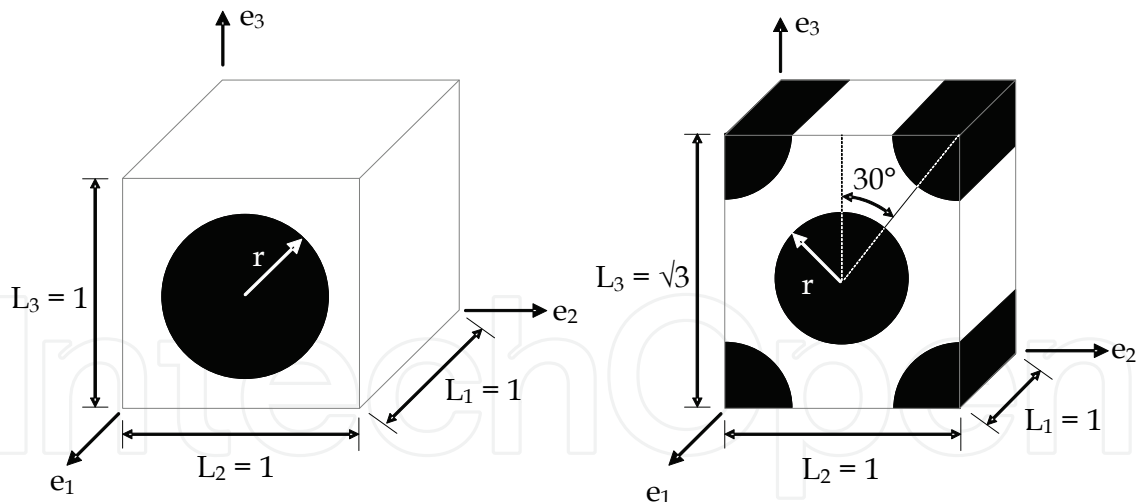

Fig. 1. Schematics of the square and hexagonal representative volume elements (Buchanan et al., 2009)

3. De-homogenization

Utilizing classical laminate theory in the analysis of a composite laminate represented as a homogenous, anisotropic solid provides accurate predictions of structural deformations resulting from applied forces and moments. Although analysts have successfully used this

approach, there are several shortcomings, which, if overcome, may provide increasingly accurate predictions of ultimate properties. The most apparent shortcomings of a homogenized analysis are: the modeling of fictitious interfaces; stresses and strains in the homogenized continuum exist in neither the fiber phase nor the matrix phase and the loss of the residual micromechanical thermal stress field due to a temperature change. The current chapter will focus on the latter two shortcomings by predicting the strain state within the fiber and matrix phases using a process referred to as micromechanical enhancement (Gosse & Christensen, 2001; Buchanan et al., 2009).

The role of micromechanical enhancement is to provide a computationally efficient micromechanics analysis that includes congruent homogenization and de-homogenization steps. The current approach uses a single finite element model subjected to canonical states of deformation to provide the information needed for both homogenization (micromechanics) and de-homogenization (micromechanical enhancement) and is thus considered to be a self-consistent approach. This chapter is primarily focused on building a general framework required to obtain self-consistent results and transferring information between micro and macro scale composite models. Through the use of a simple example problem we will address the process used to recover strains at the micro-scale resulting from both mechanical loading and residual thermal stresses.

First, consider a representative volume element subjected to an arbitrary state of average mechanical strain, $\{\bar{\varepsilon} - \bar{\alpha}\Delta T\}$, where $\bar{\varepsilon}$ is the average total strain and $\bar{\alpha}$, the vector of effective coefficients of thermal expansion for the homogenized medium. As shown in Equation 7, the state of strain at a prescribed point within the representative volume element is calculated using an influence function formulation.

$$\varepsilon_i^k - \alpha_i^k \Delta T = M_{ij}^k \left(\bar{\varepsilon}_j - \bar{\alpha}_j \Delta T \right) + A_i^k \Delta T \quad (i, j = 1-6) \tag{7}$$

The matrix M_{ij}^k and the vector A_i^k are the influence function matrix and the thermal superposition vector of strain for the kth point in the representative volume element, respectively (Gosse & Christensen, 2001; Buchanan et al., 2009).

The components of the influence function matrix can be determined uniquely, in a fashion similar to determining the stiffness matrix for the effective homogeneous medium, by prescribing a canonical state of deformation in the representative volume element and carrying out three-dimensional finite element analyses to determine the components of the strain tensor at the specified point, k. For example, let $\bar{\varepsilon}_1 \neq 0$, in the absence of the other five strain components and with no thermal loading. Shown in Equation 8, the first column of the influence matrix can be determined by relating the local strain to the average axial strain by using Equation 7.

$$\varepsilon_i^{k(\bar{\varepsilon}_1)} = M_{i1}^k \bar{\varepsilon}_1 \text{ or } M_{i1}^k = \varepsilon_i^{k(\bar{\varepsilon}_1)} / \bar{\varepsilon}_1 \quad (i = 1-6) \tag{8}$$

Note that a single finite-element analysis with boundary conditions that meet the condition, $\bar{\varepsilon}_1 \neq 0$ with $\bar{\varepsilon}_{2-6} = 0$, yields six of the 36 coefficients in the influence function matrix at any point within the representative volume element. A total of six finite-element analyses are required to completely determine terms of M_{ij}^k at any point within the domain for a given representative volume element geometry.

Calculation of the thermal superposition vector requires an additional finite element analysis in which the unit cell is subjected to a temperature change with the constraint that the average mechanical strain vanishes, i.e. $\{\bar{\varepsilon} - \bar{\alpha}\Delta T\} = 0$. Equation 9 gives the thermal superposition vector obtained by inserting this constraint into Equation 7.

$$A_i^k = \frac{\varepsilon_i^k - \alpha_i^k \Delta T}{\Delta T} \quad (i = 1 - 6) \tag{9}$$

4. Representative volume element boundary conditions

The imposition of canonical states of strain upon the representative volume element utilizing finite-element analyses requires the development of a corresponding set of displacement boundary conditions. The representative volume element principal directions, (e_1, e_2, e_3) are shown in Figure 1. Equation 10 defines the appropriate displacement boundary conditions for the prescribed extensional strain in the "1" direction with u_i representing the displacement vector and x_i the position vector.

$$u(0, x_2, x_3) = \tau_{xy}(0, x_2, x_3) = \tau_{xz}(0, x_2, x_3) = 0 \tag{10a}$$

$$u(L_1, x_2, x_3) = \bar{\varepsilon}_1 L_1; \quad \tau_{xy}(L_1, x_2, x_3) = \tau_{xz}(L_1, x_2, x_3) = 0 \tag{10b}$$

$$v(x_1, 0, x_3) = \tau_{yx}(x_1, 0, x_3) = \tau_{yz}(x_1, 0, x_3) = 0 \tag{10c}$$

$$v(x_1, L_2, x_3) = \tau_{yx}(x_1, L_2, x_3) = \tau_{yz}(x_1, L_2, x_3) = 0 \tag{10d}$$

$$w(x_1, x_2, 0) = \tau_{zx}(x_1, x_2, 0) = \tau_{zy}(x_1, x_2, 0) = 0 \tag{10e}$$

$$w(x_1, x_2, L_3) = \tau_{zx}(x_1, x_2, L_3) = \tau_{zy}(x_1, x_2, L_3) = 0 \tag{10f}$$

As an example, Equation 11 gives the canonical shearing displacements for shearing in the 2-3 plane.

$$u(0, x_2, x_3) = \tau_{xy}(0, x_2, x_3) = \tau_{xz}(0, x_2, x_3) = 0 \tag{11a}$$

$$u(L_1, x_2, x_3) = \tau_{xy}(L_1, x_2, x_3) = \tau_{xz}(L_1, x_2, x_3) = 0 \tag{11b}$$

$$w(x_1, 0, x_3) = \sigma_{yy}(x_1, 0, x_3) = \tau_{yx}(x_1, 0, x_3) = 0 \tag{11c}$$

$$w(x_1, L_2, x_3) = \bar{\gamma}_{23} L_2 / 2; \quad \sigma_{yy}(x_1, L_2, x_3) = \tau_{yx}(x_1, L_2, x_3) = 0 \tag{11d}$$

$$v(x_1, x_2, 0) = \sigma_{zz}(x_1, x_2, 0) = \tau_{zx}(x_1, x_2, 0) = 0 \tag{11e}$$

$$v(x_1, x_2, L_3) = \bar{\gamma}_{23} L_3 / 2; \quad \sigma_{zz}(x_1, x_2, L_3) = \tau_{zx}(x_1, x_2, L_3) = 0 \tag{11f}$$

This simple set of displacement boundary conditions are only valid for doubly periodic representative volume elements. In general, further constraints are required on the displacement field to maintain periodicity between adjacent unit cells. However, periodicity is satisfied automatically in the symmetric unit cells studied here. The desired average strain is recovered by inserting the boundary conditions shown in Equations 10 and 11 into Equation 6. The nodal forces taken from each face of the representative volume element can then be used in Equation 6 to determine the average stress and thereby provide the homogenized material properties as discussed in Section 2.

For the case of a uniform temperature change of the representative volume element, boundary conditions are imposed to allow for free expansion of the representative volume element with the constraint that all faces must remain planar. This condition results from Equation 8 that requires the representative volume element to exhibit the free thermal deformation $\bar{\alpha}\Delta T$ in order that the homogenized mechanical strains vanish. In this case, free thermal deformation of representative volume element is equal to that defined by the coefficients of thermal expansion of the homogenized unidirectional lamina, $\bar{\alpha}\Delta T$. The planar constraint is required to maintain periodicity between adjacent volume elements. Procedures to implement these constraints are implemented in both Abaqus (© Dassault Sytémes) and StressCheck® (ESRD). For StressCheck® when the analysis is performed for any given load, the program will create constraint equations for all the degrees of freedom associated with the selected faces. The internal degrees of freedom (faces and edges) are eliminated at the element level (local constraint equations), while the equation for the nodal variables are written in compact form at the global level.
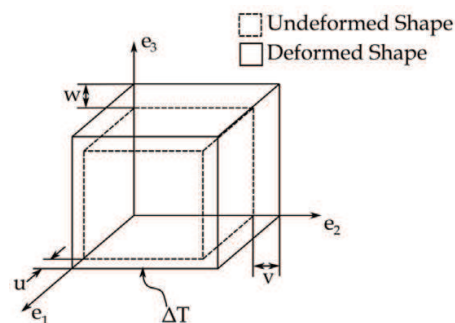

Fig. 2. Constrained deformation due to thermal loading. All faces remain planar to maintain periodicity

Since each face is constrained to remain planar, no average shearing strain will be obtained. The normal strain components are given in Equation 12. Using the normal strain components, the homogenized coefficients of thermal expansion can be determined with Equation 4, where U, V and W are the displacement components shown in Figure 2. It should be noted that these displacements are unknown prior to performing the analysis.

$$\bar{\varepsilon}_1 = \frac{U}{L_1}, \ \bar{\varepsilon}_2 = \frac{V}{L_2}, \ \bar{\varepsilon}_3 = \frac{W}{L_3} \tag{12}$$

5. Example

First, consider a general laminate to be analysed using a self-consistent micromechanics method. Presented graphically in Figure 3 is the self-consistent micromechanics method

used herein. A complete set of material properties for both the fiber and matrix phase are required. Six canonical states of deformation, extending from Equations 10 and 11, are applied as boundary conditions to two representative volume elements, a square array and a hexagonal array shown in Figure 1. The fiber volume fraction of the representative volume elements is 60 percent. For this step the finite element program Abaqus is utilized. Six canonical states of deformation provide both the homogenized stiffness matrix ($\bar{C}_{ij}$) and the enhancement matrix (M_{ij}) for the two micro-geometries.

Both domains are subjected to a uniform change in temperature in a seventh finite element analysis. This thermal loading case provides the homogenized coefficients of thermal expansion ($\bar{\alpha}_i$) and the thermal superposition vector (A_i). In total, seven finite element analyses are required for each representative volume element of interest.

The homogenized material properties become the input for the laminate level analysis. For illustration, the boundary conditions are limited to in-plane force resultants and a uniform change in temperature ΔT applied to symmetric, balanced laminates. The laminate level calculation is performed twice, once for both sets of homogenized material properties corresponding to the representative volume elements modelled.

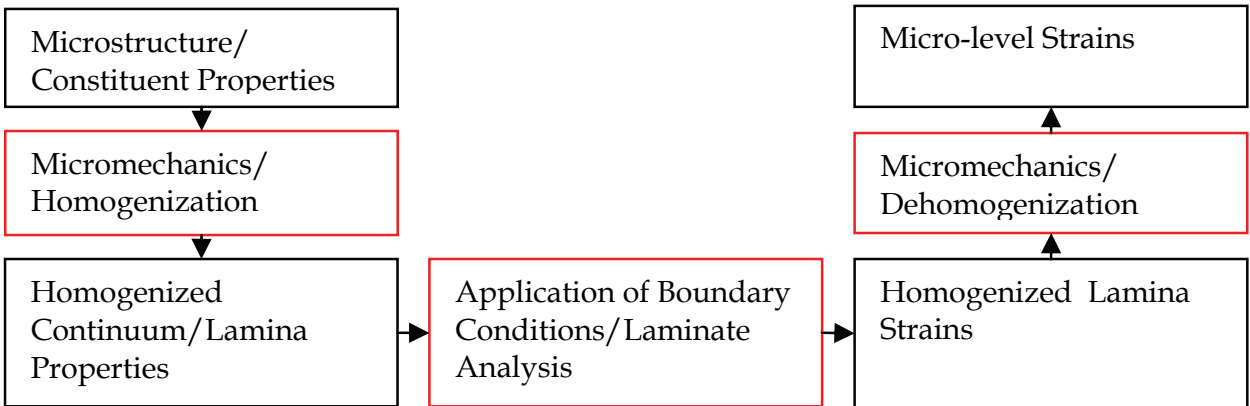| Microstructure/ Constituent Properties		Micro-level Strains
Micromechanics/ Homogenization		Micromechanics/ Dehomogenization
Homogenized Continuum/Lamina Properties	Application of Boundary Conditions/Laminate Analysis	Homogenized Lamina Strains

Fig. 3. Flow chart of self-consistent micromechanical enhancement. The analysis steps are boxed in red while the inputs and outputs to each step are boxed in black

The strains in each lamina of the laminate are calculated with a classical laminated plate theory analysis and become inputs to Equation 7. From this step, we obtain two sets of self-consistent states of strain at the micro-level, i.e. in the fiber and matrix phases. This method is considered to be a highly efficient way to obtain micro-level information because laminate geometry and loading conditions can be changed independently of the micromechanics step. Therefore, the initial set of seven finite element analyses only need to be carried out once for each representative volume element. This decoupling of micro and macro level analysis is the characteristic that is responsible for the flexibility and computational efficiency of the method described herein. The alternative approaches described in the introduction require explicit modelling of the fiber and matrix phases for each loading condition and laminate geometry.

5.1 Prediction of homogenized properties

In the current example, two representative volume elements are considered, the square and hexagonal arrays. However the self-consistent micromechanics method can be applied to other representative volume element geometries that meet the doubly periodic condition. A

schematic of each geometry is given in Figure 1. The first two columns in Table 1 are the input constituent material properties for an IM7/8552 carbon fiber, epoxy matrix composite. The final two columns in Table 1 give the predicted homogenized composite properties for the two representative volume elements.

Property	Matrix	Fiber	Square Cell	Hex Cell
E_1 (GPa)	4.76	276.0	167.5	167.5
E_2 (GPa)	4.76	19.5	11.5	10.7
E_3 (GPa)	4.76	19.5	11.5	10.7
G_{12} (GPa)	1.74	70.0	6.78	6.30
G_{13} (GPa)	1.74	70.0	6.78	6.30
G_{23} (GPa)	1.74	5.74	3.10	3.34
v_{12}	0.37	0.28	0.31	0.31
v_{13}	0.37	0.28	0.31	0.31
v_{23}	0.37	0.70	0.57	0.60
α_1 (10^{-6}/°C)	64.8	-0.4	0.41	0.41
α_2 (10^{-6}/°C)	64.8	5.6	34.7	35.1
α_3 (10^{-6}/°C)	64.8	5.6	34.7	35.1

Table 1. Fiber, matrix and equivalent homogenized medium material properties

The homogenzied stiffness matrix ($\overline{C}_{ij}$) is first calculated from Equation 3. Equation 13 shows the calculations used to determine the homogenized engineering elastic constants from the homogenzied stiffness matrix. Shown in Tables 2 and 3 are the homogenized stiffness matrix and the homogenized compliance matrix ($\overline{S}_{ij}$), respectively. The predicted engineering constants are used as inputs in the laminate level analysis.

$$\left[\overline{S}\right] = \left[\overline{C}\right]^{-1} \tag{13a}$$

$$\overline{E}_1 = 1/\overline{S}_{11}, \quad \overline{E}_2 = 1/\overline{S}_{22}, \quad \overline{E}_3 = 1/\overline{S}_{33} \tag{13b}$$

$$\overline{v}_{23} = -\overline{S}_{32}/\overline{S}_{22}, \quad \overline{v}_{13} = -\overline{S}_{31}/\overline{S}_{11}, \quad \overline{v}_{12} = -\overline{S}_{21}/\overline{S}_{11} \tag{13c}$$

$$\overline{G}_{23} = 1/\overline{S}_{44}, \quad \overline{G}_{13} = 1/\overline{S}_{55}, \quad \overline{G}_{12} = 1/\overline{S}_{66} \tag{13d}$$

Square Array, $\overline{C}_{ij}$ (GPa)						Hexagonal Array, $\overline{C}_{ij}$ (GPa)					
172.8	8.7	8.7	0.0	0.0	0.0	172.8	8.6	8.6	0.0	0.0	0.0
8.7	17.6	10.3	0.0	0.0	0.0	8.6	17.1	10.5	0.0	0.0	0.0
8.7	10.3	17.6	0.0	0.0	0.0	8.6	10.5	17.1	0.0	0.0	0.0
0.0	0.0	0.0	3.1	0.0	0.0	0.0	0.0	0.0	3.3	0.0	0.0
0.0	0.0	0.0	0.0	6.8	0.0	0.0	0.0	0.0	0.0	6.3	0.0
0.0	0.0	0.0	0.0	0.0	6.8	0.0	0.0	0.0	0.0	0.0	6.3

Table 2. Homogenized stiffness matrix representative volume elements

Square Array, $\bar{S}_{ij}$ (1/GPa 10^{-3})						Hexagonal Array, $\bar{S}_{ij}$ (1/GPa 10^{-3})					
5.97	-1.86	-1.86	0.00	0.00	0.00	5.97	-1.86	-1.86	0.00	0.00	0.00
-1.86	87.24	-50.16	0.00	0.00	0.00	-1.86	93.48	-56.07	0.00	0.00	0.00
-1.86	-50.16	87.24	0.00	0.00	0.00	-1.86	-56.07	93.48	0.00	0.00	0.00
0.00	0.00	0.00	322.27	0.00	0.00	0.00	0.00	0.00	299.00	0.00	0.00
0.00	0.00	0.00	0.00	147.54	0.00	0.00	0.00	0.00	0.00	158.69	0.00
0.00	0.00	0.00	0.00	0.00	147.54	0.00	0.00	0.00	0.00	0.00	158.69

Table 3. Homogenized compliance matrix representative volume elements

5.2 Determination of influence matrix and thermal superposition vector

The influence matrix and thermal superposition vector can be extracted from the same set finite element analyses used to determine the effective lamina properties. It should be noted that both the influence matrix and the thermal superposition vector are field variables. That is, each specific geometric point within a representative volume element yields a unique influence matrix. Presented as field variables, the terms of the influence matrices and thermal superposition vectors are illustrated graphically in Figures 4 and 5, respectively.

The micro-strain field can be extracted at every node or integration point within the representative volume element. The enhanced strain field at every point within a volume element can be used in a point failure criteria. Alternatively, a smaller set of points can be selected for examination in order to increase computational efficiency. The same method is applicable for a stress based criteria whereby the stress state at a point is determined from the strain state through the appropriate constitutive relationships.

In the current example, a single point is used to provide a numerical illustration of the micromechanical enhancement process. Tables 4 and 5 contain the influence matrix and thermal superposition vectors respectively. The data is extracted for both the square and hexagonal representative volume elements at the point $(e_1, e_2, e_3) = (L_1/2, L_2, L_3/2)$. Although both points represent locations that are midway between two fiber centers, the influence matrix and thermal superposition vectors are different for the two representative volume elements. This shows the effect of packing geometry on the local strain fields and the need for a comprehensive understanding of the underlying geometry contained in the composite material.

Square Array, M_{ij} $(x,y,z)=(0.5,1.0,0.5)$						Hexagonal Array, M_{ij} $(x,y,z)=(0.5,1.0,\sqrt{(3)}/2)$					
1.0	0.0	0.0	0.0	0.0	0.0	1.0	0.0	0.0	0.0	0.0	0.0
0.8	3.2	1.0	0.0	0.0	0.0	0.6	2.8	0.3	0.0	0.0	0.0
-0.3	-0.6	0.5	0.0	0.0	0.0	-0.2	-0.5	0.6	0.0	0.0	0.0
0.0	0.0	0.0	2.0	0.0	0.0	0.0	0.0	0.0	1.4	0.0	0.0
0.0	0.0	0.0	0.0	0.1	0.0	0.0	0.0	0.0	0.0	0.3	0.0
0.0	0.0	0.0	0.0	0.0	6.8	0.0	0.0	0.0	0.0	0.0	4.7

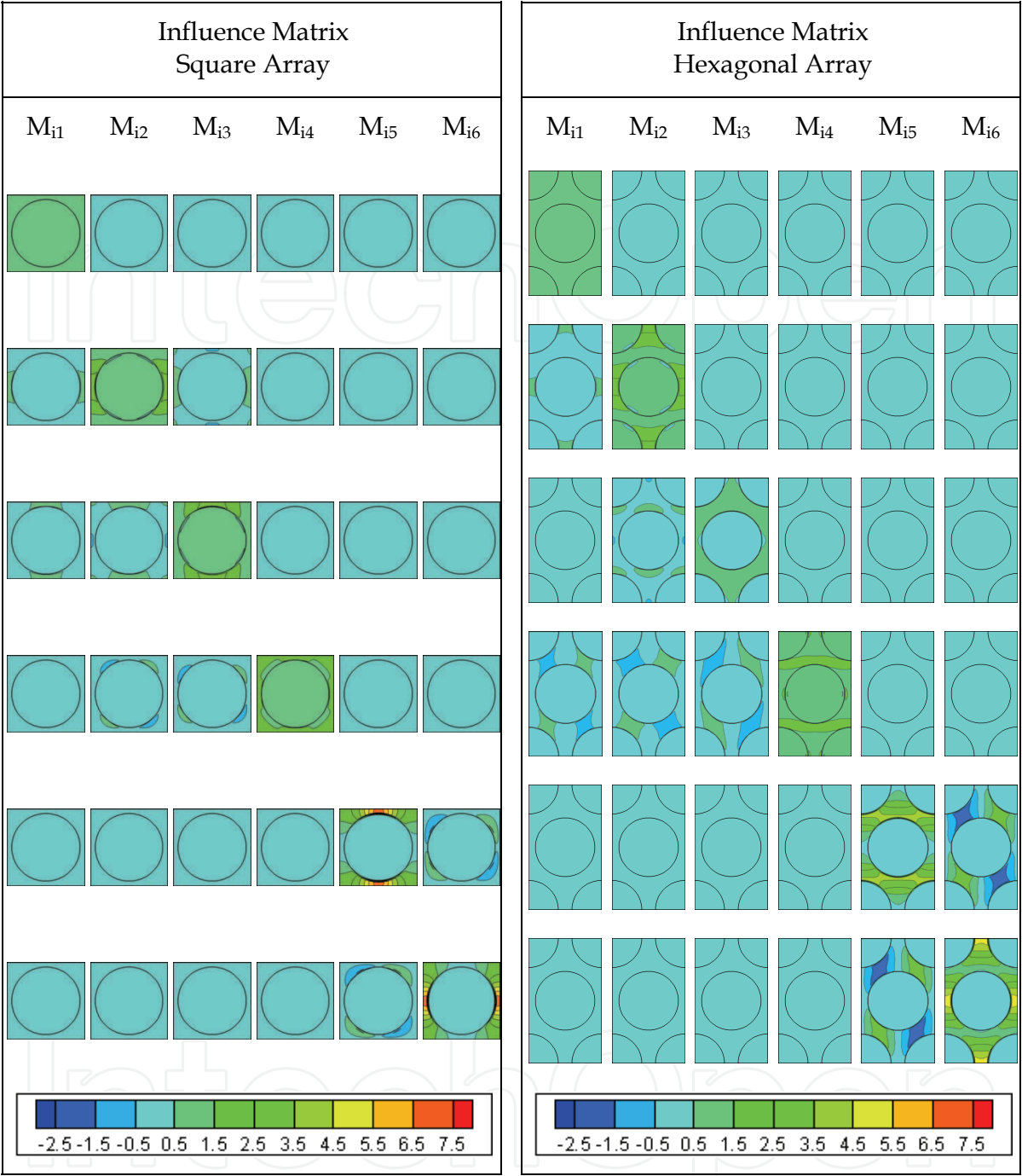Table 4. Influence matrix for both representative volume elements at the selected location

Fig. 4. Influence matrix fields for both representative volume elements, square and hexagonal

Square Array, A_i $(10^{-6}/°C)$, $(x,y,z)=(0.5,1.0,0.5)$						Hexagonal Array, A_i $(10^{-6}/°C)$, $(x,y,z)=(0.5,1.0,\sqrt{(3)}/2)$					
-64	129	-83	0	0	0	-64	90	-60	0	0	0

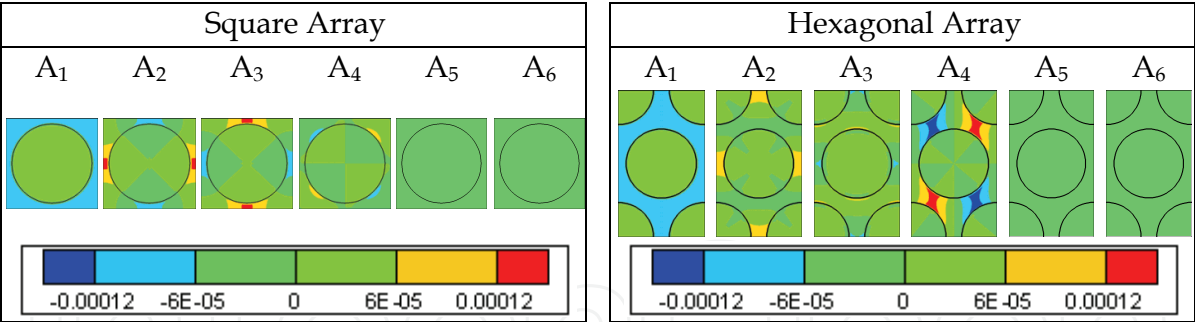Table 5. Thermal superposition vector both representative volume elements at a selected location

Fig. 5. Thermal superposition vector fields for both representative volume elements, square and hexagonal

5.3 Review of classical laminated plate theory

To illustrate the full process of using the self-consistent micromechanics method described herein, two laminate stacking sequences are investigated, the [0/90/90/0] cross-ply laminate and the [45/-45/-45/45] angle-ply laminate. For this example, the laminate level analysis is preformed using classical laminate plate theory but, finite element methods can also be used for more complex geometries and loading conditions.

Consider only the in-plane resultant forces, [N_x, N_y, N_{xy}] as defined in Figure 6, and thermal loading. Under these conditions, Equation 14 gives relationship between the lamina stresses and strains referenced to the principal material axis (1,2).

$$\bar{\sigma}_i = \bar{Q}_{ij}\varepsilon_j \ (i,j = 1,2,6) \tag{14}$$

Here, $\bar{Q}_{ij}$ is the reduced stiffness matrix in the material principal coordinate system. Equation 15 shows the entries in the reduced stiffness matrix written in terms of the homogenized stiffness matrix.

$$\bar{Q}_{ij} = \bar{C}_{ij} - \frac{\bar{C}_{i3}\bar{C}_{j3}}{\bar{C}_{33}} \ (i,j = 1,2,6) \tag{15}$$

The stresses and strains can be written in the laminate coordinate system (x,y) obtained by rotating the material coordinate system through an angle, θ, about the material 3 axis, see Figure 6. Equation 16 gives the stress strain relation of Equation 14 written in the transformed coordinate system.

$$\bar{\sigma}_i = \bar{Q}_{ij}^{'}(\varepsilon_j - \alpha_j \Delta T) \ (i,j = 1,2,6) \tag{16}$$

A primed quantity is referenced to the laminate coordinate system (x,y). As given in Equation 17, the reduced stiffness matrix referenced to the laminate coordinate system (x,y) is obtained by applying a transformation to the reduced stiffness matrix of Equation 14.

$$\left[\bar{Q}^{'}\right] = \left[T\right]^{T}\left[\bar{Q}\right]\left[T\right] \text{ with } \left[T\right] = \begin{bmatrix} c^2 & s^2 & sc \\ s^2 & c^2 & -sc \\ -2sc & 2sc & c^2-s^2 \end{bmatrix} \tag{17a, b}$$

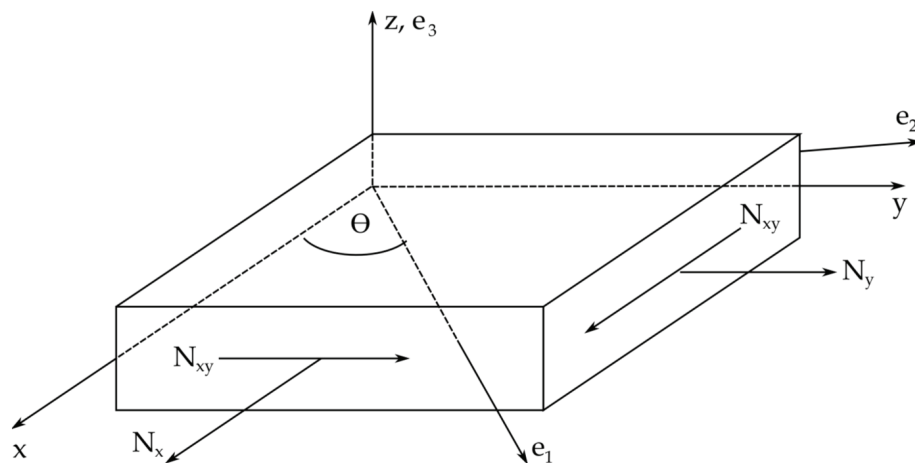$$s = \sin\theta \text{ and } c = \cos\theta \tag{17c, d}$$

Fig. 6. Definition of laminate resultant forces

For both the cross-ply and the angle-ply laminates being considered, the in-plane loading is decoupled from any out of plane curvatures. As shown in Equation 18, the laminate strains are related to the force resultants, [N_x, N_y, N_{xy}], through the extensional stiffness matrix A_{ij}.

$$\{N\} = A_{ij}\bar{\varepsilon}_j - \{N^T\}$$ (18a)

$$A_{ij} = \sum_{l=1}^{L}\left(\bar{Q}'_{ij}\right)^{(l)} t^{(l)} \text{ and } \{N^T\} = \Delta T \sum_{l=1}^{L}\left[\bar{Q}'\right]^{(l)}\{\bar{\alpha}'\}^{(l)} t^{(l)}$$ (18b,c)

Where the l index sums over the total number of lamina in the laminate and t is the thickness of each lamina. The laminate strains are determined in Equation 19 by rearranging Equation 18a.

$$\bar{\varepsilon}'_i = A_{ij}^{-1}\left[\{N\} + \{N^T\}\right]$$ (19)

For the de-homogenization step, the components of homogenized strain field must be referenced to the principal material axis. This is accomplished by applying the transformation matrix of Equation 17b to the laminate strain in Equation 19. The transformation is applied for each lamina within the laminate. The plane stress condition is then inserted into Equation 2 to determine the out-of-plane strain component, $\bar{\varepsilon}_3$. Equation 20 gives the relationships obtained for an orthotropic material system. The homogenized strain state is now fully specified and the strain state within each representative volume element can be determined.

$$\bar{\varepsilon}_3 = -\frac{\bar{C}_{13}\bar{\varepsilon}_1 + \bar{C}_{23}\bar{\varepsilon}_2}{\bar{C}_{33}}$$ (20)

5.4 Application of uniaxial force resultant, N_x

First, a purely mechanical loading is considered. The lamina level homogenized material properties calculated in Section 5.3 are used to determine the macroscopic state of strain in a

both laminates subjected an axial force resultant, N_x, in the absence of other two force resultants, N_y and N_{xy}. The laminate resultants are defined in Figure 4.

Consider the cross-ply and angle-ply laminates under a loading case in which the resulting edge forces are [Nx, Ny, Nxy] = [100 kN/m, 0, 0] without a temperature change. The macroscopic strain state in each lamina is determined using the process described in Section 5.3 with a lamina thickness, t, of 0.2 mm. The homogenized mechanical strains in the cross-ply and angle-ply laminates are given in Tables 6 and 7 respectively. From these homogenized states of strain, the state of strain within both representative volume elements is found by applying the influence matrices according to Equation 8. For this example, the influence matrices shown in Table 4 are used to determine the strain in the matrix phase at the location $(e_1, e_2, e_3) = (L_1/2, L_2, L_3/2)$. Tables 8 and 9 list the strains within the matrix at the selected point for the cross-ply and angle-ply laminates, respectively. The results show that the state of strain at the point of inquiry in each representative volume element can be very different from the homogenized state of strain in each lamina.

5.5 Application of uniform temperature change, ΔT

Next, consider the cross-ply and angle-ply laminates subjected to a uniform temperature change of ΔT = -100 °C. The macroscopic strain state in each lamina is determined using the classical laminate theory analysis outlined in Section 5.3 with a lamina thickness, t, of 0.2 millimetres. The homogenized mechanical strains in the cross-ply and angle-ply laminates are given in Tables 10 and 11 respectively. The strain within both representative volume element is found from the homogenized states of strain by applying the influence matrices and thermal superposition vectors according to Equation 8. Mechanical strains are present at the lamina level and at the micro-level for the thermal loading case. This is due to a mismatch in the homogenized coefficients of thermal expansion of the lamina and a mismatch in the coefficients of thermal expansion of the constituents. Again, the influence matrices shown in Table 4 and the thermal superposition vectors of Table 5 are used to determine the strain in the matrix phase at the location (x, y, z) = (Lx/2, Ly, Lz/2) for both representative volume elements. Tables 12 and 13 list the strain state at the selected location within the matrix for the cross-ply and angle-ply laminates, respectively. It is obvious that identical results are obtained for the [0/90/90/0] and [45/-45/-45/45] laminates because the two laminates thermally identical after a rotation of 45°. As such, both laminates have identical states of strain in the material principal coordinates.

	Square Array, 10⁻⁶		Hexagonal Array, 10⁻⁶	
	0° Ply	90° Ply	0° Ply	90° Ply
$\bar{\varepsilon}_1 - \bar{\alpha}_1 \Delta T$	1,390	-55	1,396	-52
$\bar{\varepsilon}_2 - \bar{\alpha}_2 \Delta T$	-55	1,390	-52	1,396
$\bar{\varepsilon}_3 - \bar{\alpha}_3 \Delta T$	-655	-786	-670	-825

Table 6. Homogenized mechanical strains due to a force resultant, N_x = 100 k N/m in the [0/90/90/0] laminate

	Square Array, 10⁻⁶		Hexagonal Array, 10⁻⁶	
	45° Ply	-45° Ply	45° Ply	-45° Ply
$\bar{\varepsilon}_1 - \bar{\alpha}_1 \Delta T$	667	667	672	672
$\bar{\varepsilon}_2 - \bar{\alpha}_2 \Delta T$	667	667	672	672
$\bar{\varepsilon}_3 - \bar{\alpha}_3 \Delta T$	-720	-720	-748	-748
$\bar{\varepsilon}_6 - \bar{\alpha}_6 \Delta T$	-9221	9221	-9921	9921

Table 7. Homogenized mechanical strains due to a force resultant, $N_x = 100$ kN/m in the [45/-45/-45/45] laminate

	Square Array, 10⁻⁶ $(x,y,z) = (0.5, 1.0, 0.5)$		Hexagonal Array, 10⁻⁶ $(x,y,z) = (0.5, 1.0, \sqrt{(3)}/2)$	
	0° Ply	90° Ply	0° Ply	90° Ply
$\varepsilon_1 - \alpha_1 \Delta T$	1,390	-55	1,396	-52
$\varepsilon_2 - \alpha_2 \Delta T$	281	3618	491	3,630
$\varepsilon_3 - \alpha_3 \Delta T$	-712	-1211	-655	-1,183

Table 8. Micro-level mechanical strain due to a force resultant, $N_x = 100$ kN/m at the selected location in the [0/90/90/0] laminate

	Square Array, 10⁻⁶ $(x,y,z) = (0.5, 1.0, 0.5)$		Hexagonal Array, 10⁻⁶ $(x,y,z) = (0.5, 1.0, \sqrt{(3)}/2)$	
	45° Ply	-45° Ply	45° Ply	-45° Ply
$\varepsilon_1 - \alpha_1 \Delta T$	667	667	672	672
$\varepsilon_2 - \alpha_2 \Delta T$	1,948	1,948	2060	2060
$\varepsilon_3 - \alpha_3 \Delta T$	-960	-960	-919	-919
$\varepsilon_6 - \alpha_6 \Delta T$	-62,703	62,703	-46,629	46,629

Table 9. Micro-level mechanical strain due to a shell edge traction, $N_x = 100$ k N/m at the selected location in the [45/-45/-45/45] laminate

	Square Array, 10⁻⁶		Hexagonal Array, 10⁻⁶	
	0° Ply	90° Ply	0° Ply	90° Ply
$\bar{\varepsilon}_1 - \bar{\alpha}_1 \Delta T$	-277	-277	-263	-263
$\bar{\varepsilon}_2 - \bar{\alpha}_2 \Delta T$	3,152	3,152	3,206	3,206
$\bar{\varepsilon}_3 - \bar{\alpha}_3 \Delta T$	-1,708	-1,708	-1,823	-1,823

Table 10. Homogenized mechanical strains due to thermal loading, $\Delta T = -100$ °C in the [0/90/90/0] laminate

	Square Array, 10⁻⁶		Hexagonal Array, 10⁻⁶	
	45° Ply	-45° Ply	45° Ply	-45° Ply
$\bar{\varepsilon}_1 - \bar{\alpha}_1\Delta T$	-277	-277	-263	-263
$\bar{\varepsilon}_2 - \bar{\alpha}_2\Delta T$	3,152	3,152	3,206	3,206
$\bar{\varepsilon}_3 - \bar{\alpha}_3\Delta T$	-1,708	-1,708	-1,823	-1,823

Table 11. Homogenized mechanical strains due to thermal loading, ΔT = -100 °C in the [45/-45/-45/45] laminate

	Square Array, 10⁻⁶ $(x,y,z) = (0.5, 1.0, 0.5)$		Hexagonal Array, 10⁻⁶ $(x,y,z) = (0.5, 1.0, \sqrt{(3)}/2)$	
	0° Ply	90° Ply	0° Ply	90° Ply
$\varepsilon_1 - \alpha_1\Delta T$	6123	6123	6137	6137
$\varepsilon_2 - \alpha_2\Delta T$	-4743	-4743	-728	-728
$\varepsilon_3 - \alpha_3\Delta T$	5638	5638	3356	3356

Table 12. Micro-level mechanical strain due to thermal loading, ΔT = -100 °C at the selected location in the [0/90/90/0] laminate

	Square Array, 10⁻⁶ $(x,y,z) = (0.5, 1.0, 0.5)$		Hexagonal Array, 10⁻⁶ $(x,y,z) = (0.5, 1.0, \sqrt{(3)}/2)$	
	45° Ply	-45° Ply	45° Ply	-45° Ply
$\varepsilon_1 - \alpha_1\Delta T$	6123	6123	6137	6137
$\varepsilon_2 - \alpha_2\Delta T$	-4743	-4743	-728	-728
$\varepsilon_3 - \alpha_3\Delta T$	5638	5638	3356	3356

Table 13. Micro-level mechanical strain due to thermal loading, ΔT = -100 °C at the selected location in the [45/-45/-45/45] laminate

6. Conclusions

A computationally efficient method for estimating the microscopic strain field within the discrete phases of a heterogeneous medium consisting of collimated, continuous fibers within an isotropic matrix has been developed. The goal of the development has been to provide an essential link in a multi-scale analysis of a composite structure. The structural loading and deformations at the macro-scale can be related to the state of strain within the fiber and matrix phases at the micro scale by using the self-consistent micromechanics method. The model utilizes a conventional influence function formulation and considers thermo-mechanical deformations. Results have been presented that illustrate the utility of the approach in determining microscopic state of strain in the [0/90/90/0] and [45/-45/-

45/45] laminates. Enhanced strain components within each of the lamina were calculated for both uniaxial loading and a uniform change in temperature.

The present example showed results extracted for a single point within the representative volume element. As shown in Figure 3, the influence matrix and thermal superposition vector are field values. Therefore, the state of strain within the representative volume element can also be represented as a field value. As such, the analysis is not limited to analysis of the state of strain at a single point. However, the reader may choose as many interrogation points as are required in order to address de-homogenization of all of the phases or to meet a specific need with a minimum computational cost.

Microstructures found in fiber reinforced composites typically consist of an irregular array of fibers which differ from the representative volume elements analysed herein. An efficient method for dealing with variability is through the use of a statistically equivalent periodic unit cell. With this approach, a computational step is used to generate an equivalent representative volume element that replaces the actual complex geometry. This method has been applied at several length scales including a unidirectional fiber tow (Zeman and Sejnoha, 2007).

The main assumption implicit in the analysis is that the representative volume element is subjected to a uniform state of strain. Certainly, this is not true at all locations within a laminate. Examples include areas with large strain gradients or locations with discontinuities in the assumed periodicity such as ply interfaces. In light of these limitations, the described method provides a reasonable first order approximation of the state of strain within the constitutive phases of an ordered heterogeneous medium.

7. References

Buchanan, D. L.; Gosse, J. H.; Wollschlager, J. A.; Ritchey, A. & Pipes, R. B. (2009). Micromechanical enhancement of the macroscopic strain state for advanced composite materials. *Composites Science and Technology*, Vol. 69, (month and year of the edition) page numbers (1974–1978), 0266-3538

Christensen, R. M. (1979). *Mechanics of Composite Materials*, John Wiley & Sons, 0-471-05167-5, New York, New York.

Daniel, I. M. & Ishai, O. (2006). *Engineering Mechanics of Composite Materials*, Oxford University Press, 0-19-515097, New York, New York.

Gosse, J.H. & Christensen, S. (2001). Strain Invariant Failure Criteria for Polymers in Composites. *Proceedings of 42nd AIAA/ASME/ASCE/AHS/ASC Structures, Structural Dynamics, and Materials Conference and Exhibit*, Seattle WA, April 2001

Halpin, J. C. & Tsai, S. W. (1967). Effects of Environmental Factors on Composite Materials. *Air Force Technical Report AFML-TR-67-423*, Wright Aeronautical Labs, Dayton, OH

Hashin, Z. & Rosen, B. W. (1964). The Elastic Moduli of Fiber-Reinforced Materials. *Journal of Applied Mechanics*, Vol. 21 (1964) page numbers (233-242), 0021-8936

Hashin, Z. (1972). *Theory of Fiber Reinforced Materials*. NASA CR-1974, Langley Research Center

Hill, R. (1963). Elastic Properties of Reinforced Solids: Some Theoretical Principles. *Journal of Mechanics and Physics of Solids*, Vol. 11, No. 5, (September 1963) page numbers (357-372), 0022-5096

Hill, R. (1965). Theory of Mechanical Properties of Fibre-Strengthened Materials: III, Self-Consistent Model. *Journal of the Mechanics and Physics of Solids*, Vol. 13, No. 4, (August 1965) page numbers (189-198), 0022-5096

Hutapea, P.; Yuan, F.G.; Pagano, N.J. (2003) Micro-stress prediction in composite laminates with high stress gradients. *International Journal of Solids and Structures*, Vol. 40, No. 9, (May 2003) page numbers (2215–2248), 0020-7683

Pagano, N. J. & Rybicki, E. F. (1974). On the significance of effective modulus solutions for fibrous composites. *Journal of Composite Materials*, Vol. 8, No. 3, (July 1974) page numbers (214-228), 0021-9983

Pagano, N. J. & Yuan, F. G. (2000). The significance of effective modulus theory (homogenization) in composite laminate mechanics. *Composites Science and Technology*, Vol. 60, No. 12-13, (September 2000) page numbers (2471-2488), 0266-3538

Paul, B. (1960). Prediction of Elastic Constants of Multiphase Materials. *Transactions of AIME*, Vol. 218, page numbers (36-41), 0096-4778

Pindera, M. J.; Khatam, H.; Drago, A. S. & Bansal, Y. (2009). Micromechanics of spatially uniform heterogeneous media: A critical review and emerging approaches. *Composites Part B: Engineering*, Vol. 40, No. 5, (July 2009) page numbers (349-378), 1359-8368

Raghavan, P.; Moorthy, S.; Ghosh, S. & Pagano, N. J. (2001). Revisiting the composite laminate problem with and an adaptive multi-level computational model. *Composite Science and Technology*, Vol. 61, 2001, (June 2001) page numbers (1017-1040), 0266-3538

Reuss, A. (1929). "Berechnung der Fließgrenze von Mischkristallen auf Grund der Plastizitätsbedingung für Einkristalle". *Zeitschrift für Angewandte Mathematik und Mechanik*,Vol. 9 No. 1 (February 1929) page numbers (49–58), 1521-4001

Sun, C. T. & Vaidya, R. S. (1996). Prediction of composite properties from a representative volume element. *Composites Science and Technology*, Vol. 56, No. 2, (1996) page numbers (171-179), 0266-3538

Voigt, W. (1887). Theoretische Studien über die Elasticitätsverhältnisse der Krystalle. *Abhandlungen der Gesellschaft der Wissenschaften zu Göttingen*, Vol. 34, (August 1887) page numbers (3–51)

Wang, Y.; Sun, C.; Sun, X. & Pagano, N. J. (2002). Principles for Recovering Micro-Stress in Multi-Level Analysis, In: *Composite Materials: Testing, Design and Acceptance Criteria, ASTM STP 1416*, A. Zureick and A. T. Nettles, (Ed.), page numbers (200-211), American Society for Testing and Materials International, 0-8031-2893-2, West Conshohocken, PA

Zeman, J; Sejnoha, M. (2007). From random microstructures to representative volume elements. *Modeling and Simulation in Materials Science and Engineering*, Vol. 15, No. 4, (2007) page numbers (S325-S335), 0965-0393
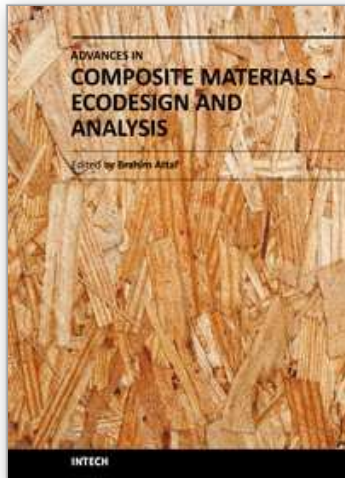
Advances in Composite Materials - Ecodesign and Analysis

Edited by Dr. Brahim Attaf

By adopting the principles of sustainable design and cleaner production, this important book opens a new challenge in the world of composite materials and explores the achieved advancements of specialists in their respective areas of research and innovation. Contributions coming from both spaces of academia and industry were so diversified that the 28 chapters composing the book have been grouped into the following main parts: sustainable materials and ecodesign aspects, composite materials and curing processes, modelling and testing, strength of adhesive joints, characterization and thermal behaviour, all of which provides an invaluable overview of this fascinating subject area. Results achieved from theoretical, numerical and experimental investigations can help designers, manufacturers and suppliers involved with high-tech composite materials to boost competitiveness and innovation productivity.

How to reference

In order to correctly reference this scholarly work, feel free to copy and paste the following:

Andrew Ritchey, Joshua Dustin, Jonathan Gosse and R. Byron Pipes (2011). Self-Consistent Micromechanical Enhancement of Continuous Fiber Composites, Advances in Composite Materials - Ecodesign and Analysis, Dr. Brahim Attaf (Ed.), ISBN: 978-953-307-150-3, InTech, Available from: http://www.intechopen.com/books/advances-in-composite-materials-ecodesign-and-analysis/self-consistent-micromechanical-enhancement-of-continuous-fiber-composites

INTECH
open science | open minds